crystals

MDPI

Article

Two New Energetic Hexagonal *Anti*-Perovskites $(N_2H_5)_3X[B_{12}H_{12}] \cdot H_2O$ ($X^- = [NO_3]^-$ and $[ClO_4]^-$): Crystal Structure, Vibrational Spectra, and Thermal Decomposition

Rouzbeh Aghaei Hakkak [1], Thomas M. Klapötke [2] and Thomas Schleid [1,*]

[1] Institute for Inorganic Chemistry, University of Stuttgart, Pfaffenwaldring 55, D-70569 Stuttgart, Germany; rouzbeh.aghaei-hakkak@iac.uni-stuttgart.de
[2] Department of Chemistry, Ludwig-Maximilians University, Butenandtstrasse 5–13, D-81377 Munich, Germany
* Correspondence: schleid@iac.uni-stuttgart.de

Abstract: Two novel energetic *anti*-perovskite compounds with the chemical formula $(N_2H_5)_3X[B_{12}H_{12}] \cdot H_2O$, where X^- is either $[NO_3]^-$ or $[ClO_4]^-$, were successfully synthesized. Both dodecahydro-*closo*-dodecaborates crystallize orthorhombically in the space group $Cmc2_1$, exhibiting relatively similar lattice parameters ($(N_2H_5)_3[NO_3][B_{12}H_{12}] \cdot H_2O$: a = 915.94(5), b = 1817.45(9), c = 952.67(5) pm, $(N_2H_5)_3[ClO_4][B_{12}H_{12}] \cdot H_2O$: a = 1040.51(6), b = 1757.68(9), c = 942.34(5) pm both for Z = 4). Their synthesis involved a two-step process: first, $Cs_2[B_{12}H_{12}]$ passed through a cation exchange column to yield the acidic form of the dodecahydro-*closo*-dodecaborate, $(H_3O)_2[B_{12}H_{12}]$. This aqueous solution was subsequently neutralized with hydrazinium hydroxide and mixed with the corresponding water-dissolved hydrazinium salt (nitrate or perchlorate). Characterization of the obtained crystals was performed by single-crystal X-ray diffraction and Raman spectroscopy as well as thermal analyses (TG-DTA and DSC). The crystal structure determinations revealed that both compounds adopt a hexagonal *anti*-perovskite structure, distorted by the presence of water molecules. These compounds containing oxidizing oxoanions demonstrate a remarkable ability to release large amounts of energy (almost 2100 J/g) upon thermal decomposition.

Keywords: hydroborates; crystal structures; hydrazinium salts; *anti*-perovskites; energetic materials; thermal analyses; vibrational spectra

Citation: Aghaei Hakkak, R.; Klapötke, T.M.; Schleid, T. Two New Energetic Hexagonal *Anti*-Perovskites $(N_2H_5)_3X[B_{12}H_{12}] \cdot H_2O$ ($X^- = [NO_3]^-$ and $[ClO_4]^-$): Crystal Structure, Vibrational Spectra, and Thermal Decomposition. *Crystals* **2024**, *14*, 310. https://doi.org/10.3390/cryst14040310

Academic Editor: Maria Gazda

Received: 22 February 2024
Revised: 15 March 2024
Accepted: 19 March 2024
Published: 27 March 2024

1. Introduction

Energetic materials were initially discovered around 220 BC [1], but their need significantly surged after the industrial revolution. This rapid growth in demand can be attributed to the wide-ranging applications of these materials in the new industrial world, including their use in mining [2], construction and demolition [3], propellants [4], oil and gas exploration [5], and pyrotechnics [6], among others. Hydrazine (diamine or diazane), characterized by a single nitrogen–nitrogen bond, serves multiple roles in the field of energetic materials, including functioning as a primary explosive, as seen in the case of nickel hydrazinium nitrate [7], and as a propellant for spacecrafts [8], in addition to its use in pyrotechnics [9]. Anhydrous hydrazine is a challenging chemical to handle, primarily due to its array of hazardous properties. These properties include high toxicity, the potential for vapor-phase flammability, and the risk of detonation even in the absence of air. As a result, working with anhydrous hydrazine demands specialized training and the use of sophisticated equipment [10]. Neutral hydrazine can be protonated to form $(N_2H_5)^+$ and subsequently used as cation to create various salts. Examples of such ionic salts include hydrazinium nitrate [11] and hydrazinium perchlorate [12].

On the other hand, hydroborates, particularly dodecahydro-*closo*-borate $[B_{12}H_{12}]^{2-}$, have been well-known since 1960 [13]. The compounds and derivatives of these hydro-

borates have attracted many researchers due to their unique properties [14]. Alkali- and alkaline-earth metal compounds featuring $[B_{12}H_{12}]^{2-}$ as a counter-anion have demonstrated relatively high stability across a broad temperature range. For instance, $Cs_2[B_{12}H_{12}]$ [15] and $Cs_3Cl[B_{12}H_{12}]$ remain solid and stable up to temperatures of around 700 and 900 °C, respectively. Recent developments in the field of energetic hydro-*closo*-borate compounds in combination with hydrazinium like $(N_2H_5)_2[B_{10}H_{10}]$ [16] and $(N_2H_5)_2[B_{12}H_{12}]$ [17] have shown promise for further research. Since they exhibit significant energy release during their thermal decomposition. For instance, $(N_2H_5)_2[B_{10}H_{10}] \cdot 2\ N_2H_4$ and $(N_2H_5)_2[B_{12}H_{12}] \cdot 2\ N_2H_4$ release approximately 2300 and 1600 J/g, respectively [16], upon decomposition under inert gas atmosphere (N_2). This energy release makes them noteworthy candidates for further studies in the field of energetic materials.

Perovskite materials made their debut in 1839 with the discovery of $CaTiO_3$ [18], marking a pivotal moment in the field. This landmark event laid the groundwork for extensive research and exploration in the domain of oxide-based materials. Even today, perovskites remain one of the most actively studied subjects in the realm of chemistry [19], thanks to their versatility and a wide array of applications that range from photovoltaics [20] to sensor materials [21]. In contrast, *anti*-perovskite materials share the same elemental composition as perovskites, but with an inverse charge arrangement. Unlike perovskites, which typically feature a divalent and a tetravalent cation such as calcium and titanium, *anti*-perovskites incorporate two negatively charged anions of different size, resulting in an altered charge distribution pattern [22]. Previous research on dodecahydro-*closo*-dodecaborates and the synthesis of various *anti*-perovskite compounds, such as luminescent $Tl_3Cl[B_{12}H_{12}]$ [23], $K_3Br[B_{12}H_{12}]$ [24], $Cs_3[BH_4][B_{12}H_{12}]$ [25], and in the latest research $Cs_3X[B_{12}H_{12}]$ (X^- = $[NO_3]^-$, $[ClO_3]^-$ and $[ClO_4]^-$), as the first energetic *anti*-perovskites synthesized and characterized [26] has shown their unique properties as they remain intact until temperatures around 330 °C and are capable of releasing about 2000 J/g. These studies have demonstrated their suitability as large divalent anions for the synthesis of *anti*-perovskite compounds. Despite the extensive body of research on applications and properties of perovskite and *anti*-perovskite materials, the investigation of energetic perovskites remains relatively limited in comparison to other topics [27–29]. These energetic perovskites (ABX_3) are characterized by the presence of a monovalent cation, such as sodium or ammonium, at the *A*-site, a divalent cation, like diprotonated diamines, at the *B*-site, and a strong oxidizer, such as nitrate or perchlorate, at the *X*-site. In contrast, energetic *anti*-perovskite compounds exhibit a different composition. In the presented compounds, the *A*- and *X*-sites contain energetic materials and fuels such as $(N_2H_5)^+$ and $[B_{12}H_{12}]^{2-}$, and on the *B*-site, the oxidizer is located to result in $(N_2H_5)_3[NO_3][B_{12}H_{12}]$ or $(N_2H_5)_3[ClO_4][B_{12}H_{12}]$. This arrangement differs from traditional perovskite structures and is tailored to enable unique and controlled energetic properties in these materials. In this research, the crystal structure, thermal behavior, and energetic properties of the two novel compounds $(N_2H_5)_3[NO_3][B_{12}H_{12}] \cdot H_2O$ (**I**) and $(N_2H_5)_3[ClO_4][B_{12}H_{12}] \cdot H_2O$ (**II**) are analyzed with single-crystal X-ray diffraction, thermogravimetry (TG), differential scanning calorimetry (DSC), and Raman spectroscopy.

2. Materials and Methods

2.1. Synthesis

The two new *anti*-perovskite compounds featuring dodecahydro-*closo*-dodecaborate anions were obtained by dissolving $Cs_2[B_{12}H_{12}]$ (ABCR; Karlsruhe, Germany) in a minimal amount of distilled water and passing it through a 40 cm-length column filled with a cation exchange membrane Amberlite® 120-IR (Sigma-Aldrich; Burlington, VT, USA). Subsequently, the aqueous solution of $(H_3O)_2[B_{12}H_{12}]$ was neutralized with hydrazinium hydroxide $(N_2H_5)[OH]$ (Merck; Darmstadt, Germany). A 1:1 molar ratio of the appropriate freshly prepared hydrazinium salts [16], synthesized before by mixing hydrazinium hydroxide and 70% nitric acid (Sigma-Aldrich; Burlington, VT, USA) or perchloric acid (70%, Fisher Scientific; Waltham, MA, USA), was added to portions of this solution (Figure 1). The

resulting clear brines were subjected to isothermal evaporation at room temperature, leading to the formation of transparent and colorless single crystals of the respective hydrated salts $(N_2H_5)_3X[B_{12}H_{12}] \cdot H_2O$ (X^- = $[NO_3]^-$ and $[ClO_4]^-$).

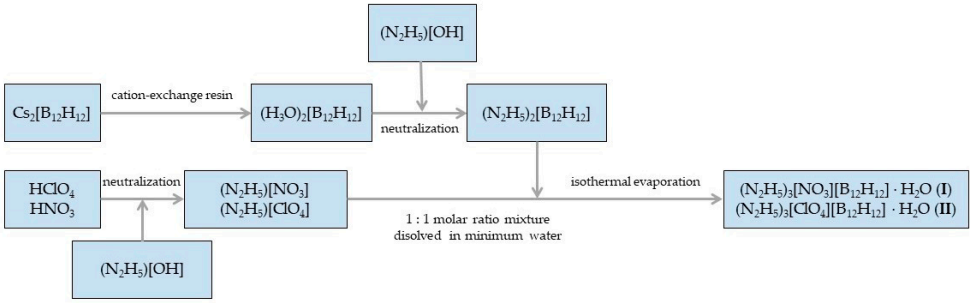

Figure 1. Synthesis flowchart for compounds (**I**) and (**II**).

2.2. Characterization Techniques

2.2.1. X-ray Crystallography

Single-crystal X-ray diffraction data were obtained using a Nonius κ-CCD diffractometer (Karlsruhe), utilizing Mo-Kα radiation that was graphite-monochromatized to a wavelength of λ = 71.07 pm. The entire process, from the initial structure solution using direct methods to subsequent structure refinement, was carried out using the SHELX-97 program [30,31]. Precise atomic positions were determined via difference Fourier maps derived from the collected data, enabling the anisotropic refinement of all non-hydrogen atoms. Detailed information on data collection and final structure refinements can be found in Table 1. Supplementary data related to structure refinements are accessible through the Fachinformationszentrum (FIZ) Karlsruhe (D-73644 Eggenstein-Leopoldshafen, E-mail: crysdata@fiz-karlsruhe.de), cross-referenced with the numbers provided in Table 1. Fractional atomic positions are additionally provided in Tables S1 and S2 of the Supplementary Material. It is noteworthy that hydrogen atom positions were determined via electron-density maps generated by difference Fourier syntheses using X-ray diffraction data. No further calculations or corrections were deemed necessary as the positions of these hydrogen atoms are well-defined based on their precise angles and distances in relation to other atoms.

Table 1. Theoretical and real amount of nitrogen and hydrogen in compounds (**I**) and (**II**).

Compound	N (Theoretical/Found) %	H (Theoretical/Found) %
$(N_2H_5)_3[NO_3][B_{12}H_{12}] \cdot H_2O$	30.54/30.48	9.11/9.09
$(N_2H_5)_3[ClO_4][B_{12}H_{12}] \cdot H_2O$	23.45/23.34	8.15/8.10

An aliquot of the samples was mounted onto a STADI-P diffractometer manufactured by Stoe & Cie (Darmstadt, Germany). Subsequently, it underwent measurement utilizing Cu-Kα radiation with a wavelength of 154.06 pm under transmission conditions. The measurement scope for the both compounds ranged from 2θ = 5 to 60°, with the objective of confirming the phase purity of the samples. The Supplementary Material contains Figures S1 and S2, where the comparison between the calculated and the sample data can be observed.

2.2.2. Raman Spectroscopy

Raman spectroscopic analyses using the DXR Smart Raman system, developed by Thermo Fisher (Waltham), were conducted, operating at an excitation wavelength of λ = 740 nm. The spectroscopic data obtained during these analyses were thoroughly examined.

2.2.3. Thermal Analysis

In this investigation, thermal analyses were conducted using two different instruments. The first instrument, a STA 449 C Jupiter by Netzsch (Selb, Germany), equipped with alumina crucibles, played a crucial role in the study. TG analysis was performed in alumina crucibles at a heating rate of 5 K min^{-1} under an argon atmosphere. The second instrument, a DSC 201 also from Netzsch (Selb, Germany), functioned as a differential scanning calorimeter with a heating rate of 5 K min^{-1} and a nitrogen flow of 20 mL min^{-1}. Samples were prepared in aluminum crucibles with a maximum temperature of 600 °C.

2.2.4. Elemental Analysis

The elemental analysis performed during our investigation aimed to determine the nitrogen and hydrogen content in both compounds in order to verify the purity of the samples using an Elementar CHNS Analyzer Vario MICRO Cube (Langenselbold, Germany). The quantities of hydrogen and nitrogen as elements, both theoretical and found in the samples, are presented in Table 1.

3. Results

3.1. Crystal Structures

The crystal structures of two newly synthesized energetic compounds, $(N_2H_5)_3[NO_3][B_{12}H_{12}] \cdot H_2O$ (**I**) and $(N_2H_5)_3[ClO_4][B_{12}H_{12}] \cdot H_2O$ (**II**) have been successfully determined and refined. Both of these compounds exhibit the same non-centrosymmetric orthorhombic space group, namely $Cmc2_1$. Furthermore, the lattice parameters for these two compounds are quite similar: a = 915.94(5) pm, b = 1817.45(9) pm, c = 952.67(5) pm for $(N_2H_5)_3[NO_3][B_{12}H_{12}] \cdot H_2O$ (**I**), and a = 1040.51(6) pm, b = 1757.68(9) pm, c = 942.34(5) pm for $(N_2H_5)_3[ClO_4][B_{12}H_{12}] \cdot H_2O$ (**II**). Additional crystallographic details for these structures can be found in Table 2, and it is worth mentioning that both needed to be refined as inversion twins.

Table 2. Crystallographic data for the crystal structures of compounds (**I**) and (**II**) and their determination.

Compound	$(N_2H_5)_3[NO_3][B_{12}H_{12}] \cdot H_2O$ (I)	$(N_2H_5)_3[ClO_4][B_{12}H_{12}] \cdot H_2O$ (II)
temperature, K	293	293
crystal system	orthorhombic	orthorhombic
space group	$Cmc2_1$ (no. 36)	$Cmc2_1$ (no. 36)
formula units, Z	4	4
a, pm	915.94(5)	1040.51(6)
b, pm	1817.45(9)	1757.68(9)
c, pm	952.67(5)	942.34(5)
D_{cal}, g cm^{-3}	1.34	1.22
V_m, cm^3 mol^{-1}	238.8(1)	259.5(1)
$\mu(MoK_\alpha)$, mm^{-1}	0.09	0.24
$F(000)$, e^-	680	752
hkl range	±(12, 23, 12)	±(13, 22, 12)
θ_{max},°	28.55	27.48
reflections measured	11,324	14,845
reflections unique	1102	1144
R_{int}, R_σ	0.087, 0.042	0.096, 0.051
R_1, wR_2	0.055, 0.144	0.045, 0.107
GooF	1.068	1.047
CSD number	2331546	2331555

For compounds (**I**) and (**II**), all the ionic species exhibit typical distances and angles. In the case of the nitrate anion, the N–O bonds show lengths ranging from 121 to 126 pm, and the O–N–O angles fall within the interval of 119 to 121° [32]. Regarding the perchlorate anion, the Cl–O bonds have lengths varying from 139 to 143 pm, and all O–Cl–O angles are

approximately 110° [33]. Similarly, for the boron cluster $[B_{12}H_{12}]^{2-}$, the B–B bonds fall into the range of 172 to 180 pm [13] and the B–H bond lengths were restricted to 110 pm with the AFIX command in the SHELXS suite [30,34] for compound (**I**), and they range from 98 to 118 pm in compound (**II**). The N–N bonds in hydrazinium cations are about 142 pm long [12] and all the N–H bonds have various lengths in a broad array from 56 to 97 pm. Both compounds crystallize with one water molecule in their formula unit, exhibiting bond lengths of *d*(Ow–Hw) = 51–62 pm and angles of about 79–85°, but further attempts to obtain anhydrous single crystals were not successful.

3.1.1. $(N_2H_5)_3[NO_3][B_{12}H_{12}] \cdot H_2O$ (**I**)

Hydrazinium nitrate dodecahydro-*closo*-dodecaborate hydrate (Figure 2) crystallizes in the orthorhombic space group $Cmc2_1$ with unit-cell parameters of a = 915.94(5), b = 1817.45(9) and c = 952.67(5) pm. Within the unit cell of this compound (**I**), there is only one crystallographically unique nitrate anion $[NO_3]^-$, which is located on the *bc* mirror plane. Additionally, there is one crystallographically unique boron-cluster $[B_{12}H_{12}]^{2-}$, which is bisected by the *bc* mirror plane. Furthermore, two distinct hydrazinium cations $(N_2H_5)^+$ are present in the crystal structure: hydrazinium 1 (N1–N2) is positioned on the *bc* mirror plane, and hydrazinium 2 (N3–N4) is situated on the glide plane along *b*.

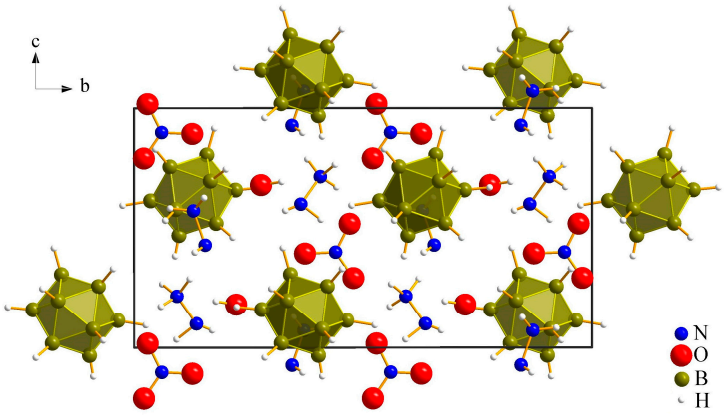

Figure 2. Extended unit-cell content of the crystal structure of $(N_2H_5)_3[NO_3][B_{12}H_{12}] \cdot H_2O$ (**I**).

The empirical formula reveals that compound (**I**) adopts an *anti*-perovskite (A_3BX) structure (Figure 3, right). In its crystal structure, each nitrate anion is surrounded by six hydrazinium cations, providing a distorted octahedral coordination environment (Figure 4), which is influenced by the presence of water molecules, exhibiting a 10.5% relative standard deviation (RSD) from the nitrogen center. Two of the faces, *trans*-oriented for each octahedron, are shared along the *c*-axis.

The crystal structure of compound (**I**) exhibits a complex network of classical hydrogen bonding interactions (Figure 3). These interactions involve hydrazinium cations, nitrate anions, and water molecules, forming a cohesive network comprising three distinct types of hydrogen bonds: hydrazinium–hydrazinium ($N^{\delta-}$–$H^{\delta+}\cdots N^{\delta-}$), hydrazinium–nitrate ($N^{\delta-}$–$H^{\delta+}\cdots O^{\delta-}$), and water–hydrazinium ($O^{\delta-}$–$H^{\delta+}\cdots N^{\delta-}$) interactions. In this complex network, each water molecule (Ow and Hw) is engaged with two crystallographically distinct hydrazinium cations. Specifically, Ow forms a hydrogen bond through H12 to N1 of hydrazinium1 (Ow···H12–N1), with a distance of 242(4) pm and an angle of 111(3)°. On the other hand, hydrazinium 2 is connected to the water molecule via Hw (N4···Ow–Hw).

The nitrate anion serves as the central node of this hydrogen-bond network with all oxygen atoms intricately connected to surrounding hydrazinium cations. For instance, O1 is linked to N1 and N4 via H12 and H41, while O2 interacts with hydrazinium 1 and hydrazinium 2 cations through H11 and H31, respectively, with nearly identical bond lengths of 228(3) and 235(4) pm, and angles of 121(4) and 120(3)°, respectively. Furthermore, O3 forms a connection with N1 via H11 (bond length: 205(5) pm; angle:

160(5)°), highlighting the intricate nature of the hydrogen-bonding interactions in this system. Finally, N2 of hydrazinium 2 is involved in hydrogen bonds with N3 of the same hydrazinium cation via H32. Detailed information regarding the bond lengths and angles of all relevant hydrogen bonds is provided in Table 3.

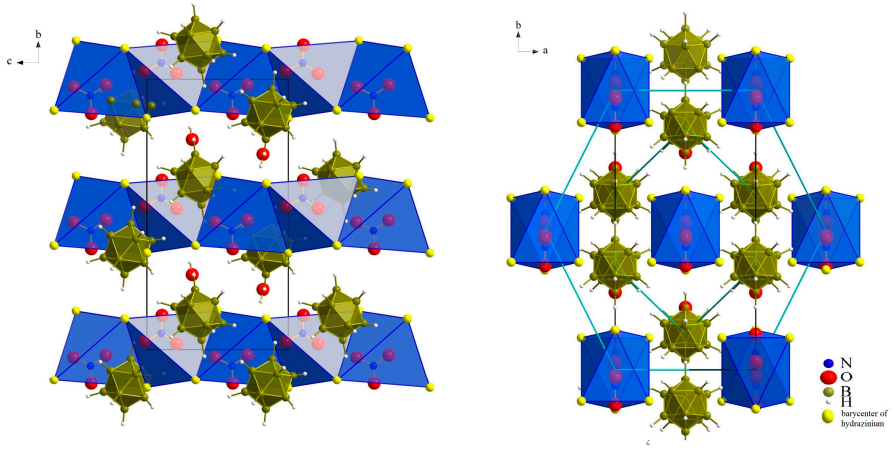

Figure 3. Distorted hexagonal *anti*-perovskite setting of $(N_2H_5)_3[NO_3][B_{12}H_{12}] \cdot H_2O$ (**I**) in two different views.

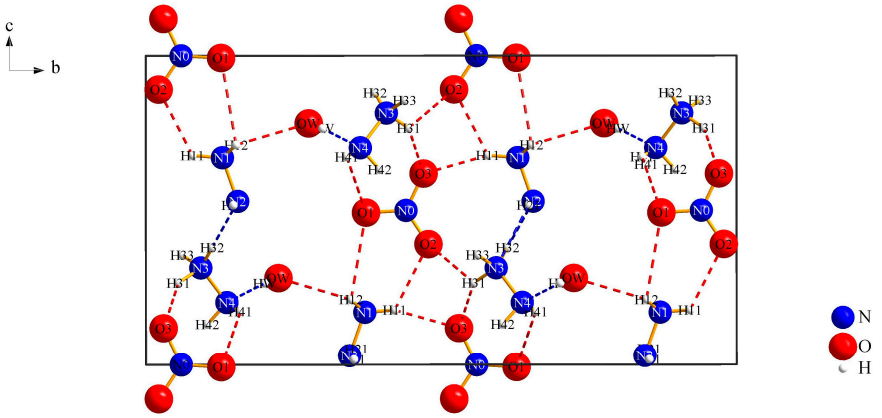

Figure 4. Illustration of the classical hydrogen-bond system in $(N_2H_5)_3[NO_3][B_{12}H_{12}] \cdot H_2O$ (**I**).

Table 3. Hydrogen bonds in the crystal structure of $(N_2H_5)_3[NO_3][B_{12}H_{12}] \cdot H_2O$ (**I**).

Interaction	Hydrogen-Bond Length (*d*/pm)	Angle (∠/°)
Ow···H12–N1	242(4)	111(3)
O1···H41–N4	284(5)	120(53)
O1···H12–N1	280(4)	99(3)
O2···H11–N1	228(6)	121(4)
O2···H31–N3	235(4)	120(3)
O3···H11–N1	205(5)	160(5)
N2···H32–N3	215(4)	177(3)
N4···Ow–Hw	218(4)	166(5)

Classical hydrogen bonding reveals another reason for the distortion of octahedra, namely that O1 has four hydrogen bonds, two to N1 and N4 via H12 and H41, and also O2 and O3 have one bond to N1 and N3 via H11 and H31, so these six bonds are holding the nitrate anions in their distorted position and not exactly in the barycenter of the polyhedron (Figure 5).

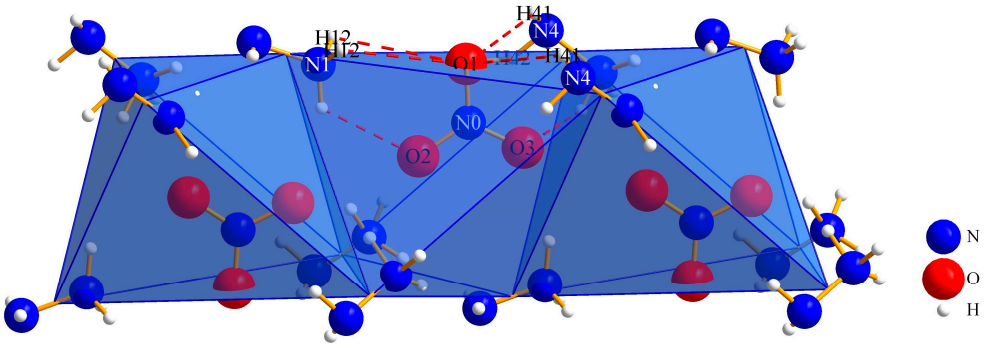

Figure 5. Face-shared setting of the octahedral environment of nitrate anions by hydrazinium cations in $(N_2H_5)_3[NO_3][B_{12}H_{12}] \cdot H_2O$ (**I**).

Another hydrogen-bonding system in this compound (**I**) (Figure 6) involves dihydrogen bonds ($N^{\delta-}$–$H^{\delta+}\cdots H^{\delta-}$–$B^{\delta+}$), which result from the interaction between the negatively polarized hydrogen atoms at the boron-cluster anions $[B_{12}H_{12}]^{2-}$ and the positively charged hydrogen atoms at the hydrazinium cations $(N_2H_5)^+$. This dihydrogen bond network contributes to the overall bonding complexity within the crystal structure. In this structural motif, each boron cluster is surrounded by ten hydrazinium cations with H···H distances ranging from 218 to 254 pm and one water molecule 245(1) pm apart. As a result, the icosahedral boron cluster exhibits a coordination number of eleven in this specific arrangement.

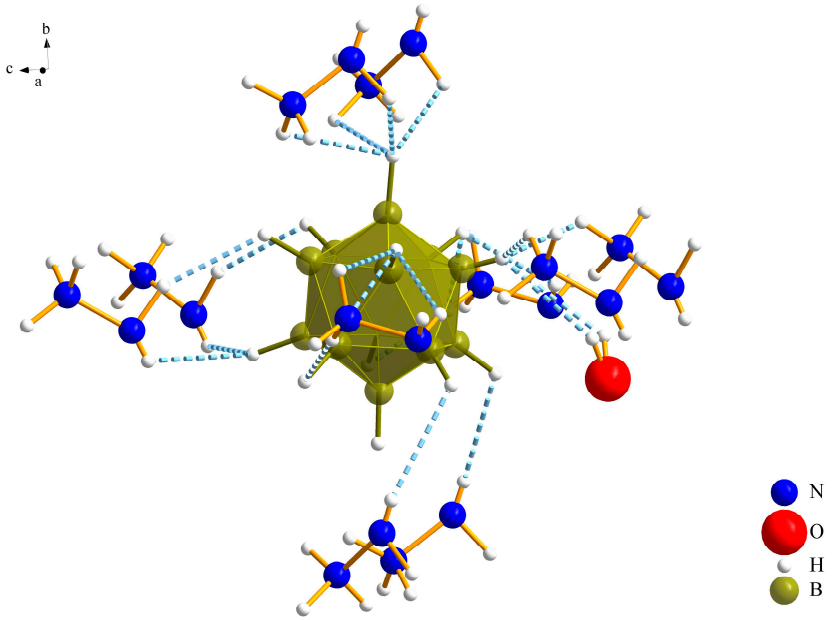

Figure 6. Dihydrogen-bonding system in $(N_2H_5)_3[NO_3][B_{12}H_{12}] \cdot H_2O$ (**I**).

3.1.2. $(N_2H_5)_3[ClO_4][B_{12}H_{12}] \cdot H_2O$ (**II**)

Hydrazinium perchlorate dodecahydro-*closo*-dodecaborate hydrate also crystallizes in the orthorhombic space group $Cmc2_1$ with the unit-cell dimensions of a = 1040.51(6), b = 1757.68(9) and c = 942.34(5) pm. Just like compound (**I**), the almost isotypic structure of compound (**II**) consists of one crystallographically distinct boron-cluster anion $[B_{12}H_{12}]^{2-}$, one perchlorate anion $[ClO_4]^-$, one water molecule H_2O, and two hydrazinium cations $(N_2H_5)^+$. The boron cluster, the perchlorate anion, the water molecule, and the hydrazinium cation of type 2 (N3–N3) are situated on the *bc* mirror plane. The crystallographic properties of hydrazinium 2 present a challenge, as each of the nitrogen atoms in these hydrazinium cations accommodates three hydrogen atoms, while one of them needs to carry only two of these to form a $(N_2H_5)^+$ cation, due to the presence of a mirror plane. The mirror

plane complicates the determination of the positions of all hydrogen atoms accurately. Consequently, the hydrazinium cation associated with the mirror plane is identified with only four hydrogen atoms in this presentation for the sake of a proper description of the hydrogen bond system. Additionally, the presence of another hydrazinium cation (hydrazinium 1: N1–N2) without any complications on the glide the plane along *b* further contributes to the intricate crystallographic nature of the compound (**II**).

Examining compound (**II**) in greater detail provides insights into the relevant polyhedra within the unit cell (Figure 7), again revealing a consistent pattern of distorted hexagonal pillars sharing faces along the crystallographic [001] direction. Despite the distortions introduced by the water molecules also in this composition, a discernible hexagonal arrangement persists.

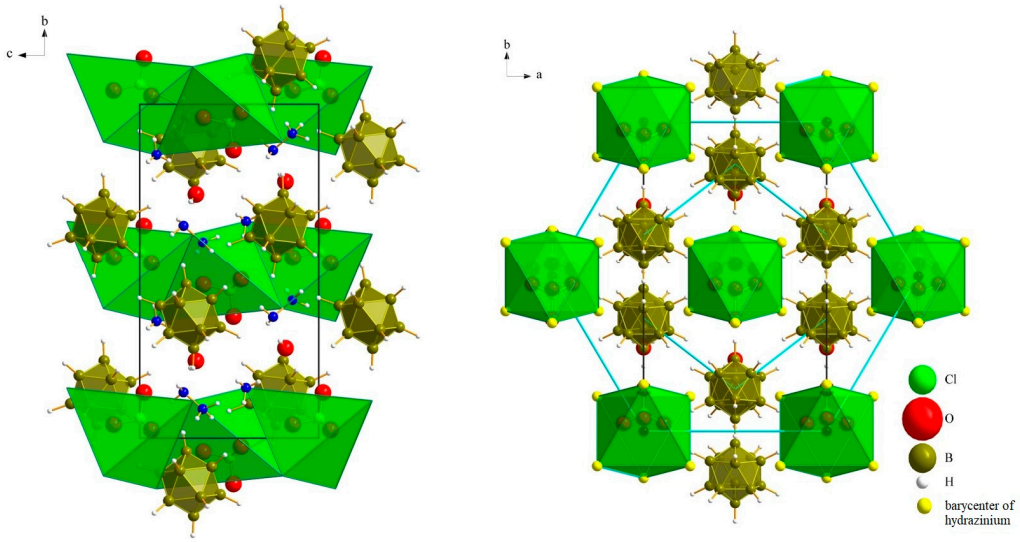

Figure 7. Distorted hexagonal *anti*-perovskite setting of $(N_2H_5)_3[ClO_4][B_{12}H_{12}] \cdot H_2O$ (**II**) in two different views.

The hydrogen-bonding network within the structure of $(N_2H_5)_3[ClO_4][B_{12}H_{12}] \cdot H_2O$ (**II**) is characterized by a complex array of interactions involving hydrazinium cations, perchlorate anions, and water molecules (Figure 8). As previously mentioned, the existence of the *bc* mirror plane makes it difficult to find proper hydrogen locations and the number of hydrogen atoms in hydrazinium 2, so the pictures of the hydrogen-bond system were created after removing H33, which has the least interaction in hydrogen bonding, but should show half-occupation (Table S2). However, the picture of the full hydrogen-bonding scheme is available as Figure S3 in the Supplementary Material. These interactions play a crucial role in stabilizing the structure and influencing the properties of compound (**II**). The hydrogen bond between O1 and Hw–Ow, with a bond length of 265(3) pm and an angle of 128(4)°, underscores the interaction between the water molecule and perchlorate anion. Similarly, the hydrogen bond between O1 and H21–N2, with a bond length of 310(4) pm and an angle of 126(4)°, highlights the interaction between perchlorate and hydrazinium. Furthermore, the interactions between O2 and H13–N1 (bond length: 225(4) pm; angle: 147(3)°) and O2 and H32–N3 (bond length: 234(5) pm; angle: 158(4)°) emphasize the involvement of hydrazinium and perchlorate in stabilizing the crystal lattice. Similarly, interactions between O3 and H13–N1 (bond length: 234(4) pm; angle: 126(3)°) and O3 and H22–N2 (bond length: 271(4) pm; angle: 111(3)°) highlight the intricate hydrogen-bonding network. Additionally, the hydrogen bond between Ow and H31–N3 (bond length: 246(6) pm, angle: 126(5)°) and between N3 and H11–N1 (bond length: 237(5) pm; angle: 166(6)°) further contribute to the structural stability of the compound. Overall, these hydrogen-bonding interactions collectively govern the structural arrangement and properties of $(N_2H_5)_3(ClO_4)[B_{12}H_{12}] \cdot H_2O$ (**II**), emphasizing the intricate interplay between

its constituent ions and molecules. The detailed bond lengths and angles of all relevant hydrogen bonds in compound (**II**) are listed in Table 4.

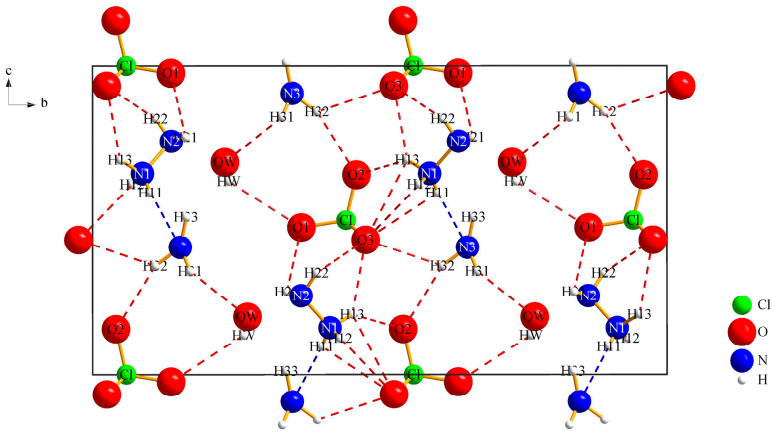

Figure 8. Sketch of the classical hydrogen-bond system in $(N_2H_5)_3[ClO_4][B_{12}H_{12}] \cdot H_2O$ (**II**).

Table 4. Hydrogen bonds in the crystal structure of $(N_2H_5)_3[ClO_4][B_{12}H_{12}] \cdot H_2O$ (**II**).

Interaction	Hydrogen-Bond Length (*d*/pm)	Angle (∠/°)
O1···Hw–Ow	265(3)	128(4)
O1···H21–N2	310(4)	126(4)
O2···H13–N1	225(4)	147(3)
O2···H32–N3	234(5)	158(4)
O3···H13–N1	234(4)	126(3)
O3···H22–N2	271(4)	111(3)
Ow···H31–N3	246(6)	126(5)
N3···H11–N1	237(5)	166(6)

In compound (**II**), similarly to compound (**I**), hydrogen bonding plays a crucial role in shaping the structure. Unlike what is expected, the perchlorate anions do not reside in the barycenter of the octahedra constructed by the $(N_2H_5)^+$ cations, but instead move closer to some of these hydrazinium units (Figure 9). This shift happens because of six specific hydrogen bonds, such as (O2···H32–N3), (O1···H21–N2), and (O3···H22–N2), each occurring twice. These hydrogen bonds essentially nudge the perchlorate anions towards the hydrazinium cations, causing them to deviate from their usual central position within the *trans*-face shared octahedral pillar.

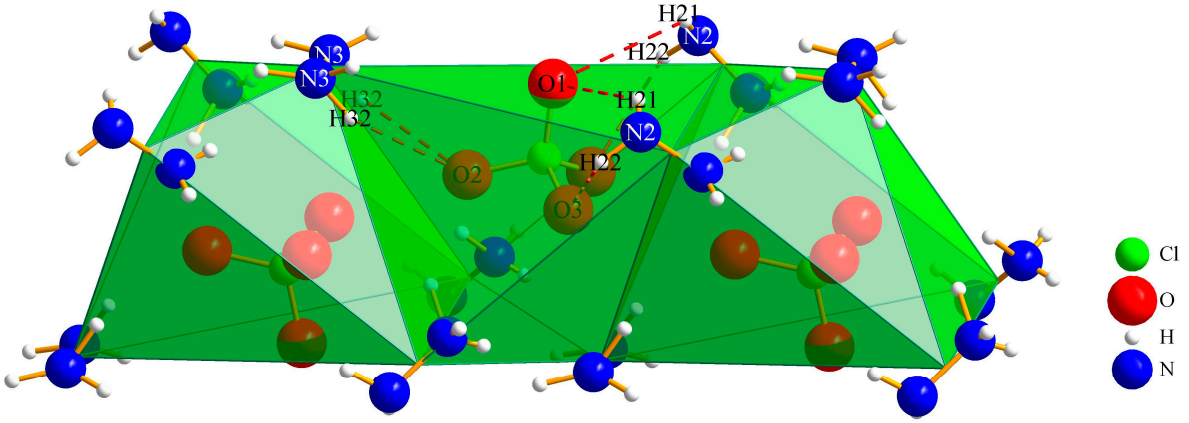

Figure 9. Face-shared setting of the octahedral environment of perchlorate anions by hydrazinium cations in $(N_2H_5)_3[ClO_4][B_{12}H_{12}] \cdot H_2O$ (**II**).

Another hydrogen-bonding system, which dominates the structure of (**II**), is created by dihydrogen bonds. As previously mentioned, these bonds result from the negatively polarized hydrogen atoms at the boron cluster and positively charged hydrogen atoms of the hydrazinium cations, and are filling the surrounding environment of the $[B_{12}H_{12}]^{2-}$ icosahedra (Figure 10) with ten hydrazinium cations and one water molecule (coordination number of eleven) with bonding ranges from 224 to 263 pm.

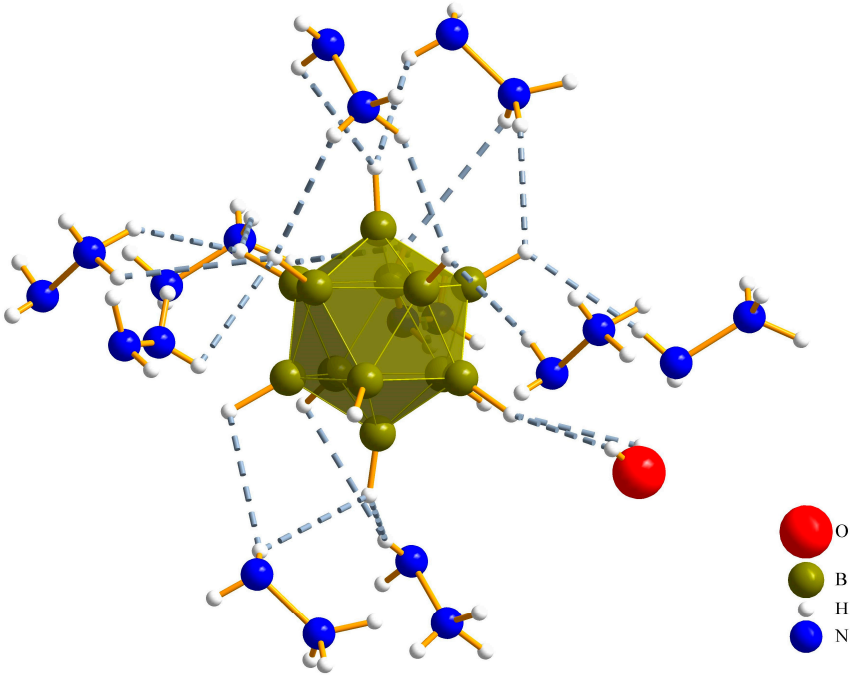

Figure 10. Dihydrogen-bonding system in $(N_2H_5)_3[ClO_4][B_{12}H_{12}] \cdot H_2O$ (**II**).

3.2. Raman Spectroscopy

Raman spectroscopy was performed on $(N_2H_5)_3[NO_3][B_{12}H_{12}] \cdot H_2O$ (**I**) and $(N_2H_5)_3[ClO_4][B_{12}H_{12}] \cdot H_2O$ (**II**) (Figure 11), revealing strong similarities in eight spectral regions for both compounds. The first region, ranging from 3200 to 3300 cm^{-1}, corresponds to the stretching vibrations of the symmetric and asymmetric N–H groups, which typically occur within this frequency range. In the subsequent region around 2400–2500 cm^{-1}, the symmetric breathing vibration of the boron cage is observed, which splits up due to dihydrogen bonding, and this vibration primarily gets influenced by the stretching mode of the B–H bonds. Weak bands in the vicinity of 1625 cm^{-1} are attributed to the deformation vibration of $–NH_3^+$ groups. Additionally, there are weak bands between 1300 and 1400 cm^{-1}, corresponding to the rocking vibration of $–NH_2$ groups. Within the 1080–1090 cm^{-1} range, the rocking vibration of $–NH_3^+$ groups become noticeable, followed by B–B skeleton vibrations around 930–960 cm^{-1}. The most intense band, found at 750 cm^{-1}, corresponds to the symmetric breathing mode of the boron cage. The seventh region, covering a range from 570 to 600 cm^{-1}, is associated with the deformation modes of B–B–H and B–B–B bonds of the $[B_{12}H_{12}]^{2-}$ icosahedra. Finally, the last region below 200 cm^{-1} results from lattice vibrations ([23,24]). For compound (**I**), the intense symmetric stretching mode of the nitrate anion is observed around 1050 cm^{-1} [35], and for compound (**II**), there are three regions around 950 cm^{-1}, which belong to the symmetric Cl–O stretching modes (which here overlap with the B–B skeleton vibrations) at wavenumbers of 620 and 470 cm^{-1}, are linked with active and inactive deformation modes of the Cl–O bonds [36], and appear as unique peaks.

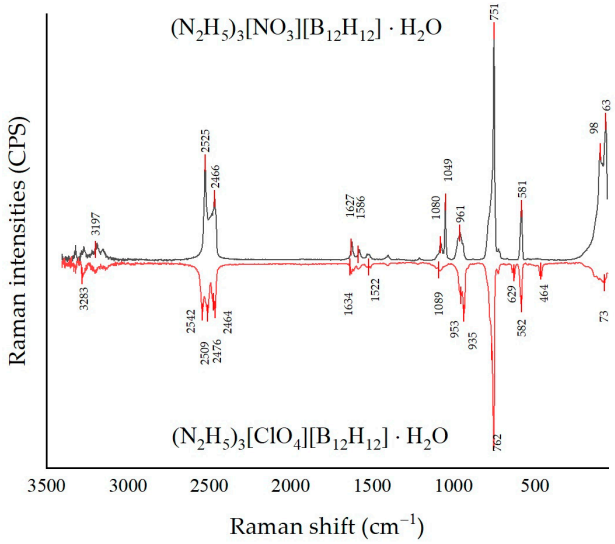

Figure 11. Raman spectra of $(N_2H_5)_3[NO_3][B_{12}H_{12}] \cdot H_2O$ (**I**) (top) and $(N_2H_5)_3[ClO_4][B_{12}H_{12}] \cdot H_2O$ (**II**) (bottom) recorded at an excitation wavelength of λ = 740 nm.

3.3. Thermal Analysis

Two different thermal analyses were conducted for compounds (**I**) and (**II**), thermogravimetry (TG) and differential scanning calorimetry (DSC). The TG analysis of these compounds (Figure 12) indicates that around 100 °C they start losing their water molecules, which is around 5% mass for compound (**I**) and about 4% for compound (**II**), while theoretically, the expected values should be 5.6 and 5.0%, respectively. The variance between these values is attributed to the inherent inability of hydrate compounds to retain their water molecules in a dry atmospheric environment, leading to gradual water losses. After that point, the anhydrous compounds remain stable until temperatures around 250 °C, from which on the entire structure starts to decompose, losing large amounts of mass, which is around 40% for compound (**I**) and 32% for compound (**II**). This contrasts to the previously described compounds $Cs_3[NO_3][B_{12}H_{12}]$ and $Cs_3[ClO_4][B_{12}H_{12}]$ [26], which have different decomposition temperatures with onset points of 322 °C for the perchlorate- and 440 °C for the nitrate-containing compound with mass losses of less than 2%, when these two compounds start their decomposition at almost the same temperature. This decomposition temperature is relatively close to the temperature, where dihydrazinium dodecahydro-*closo*-dodecaborate dihydrazinate decomposes [16], which indicates that in compounds (**I**) and (**II**), the hydrazinium cations are the primary cause of the decomposition reaction in contrast to the cesium-hydroborate *anti*-perovskites. After the second step, no other mass loss can be observed until a temperature of 500 °C.

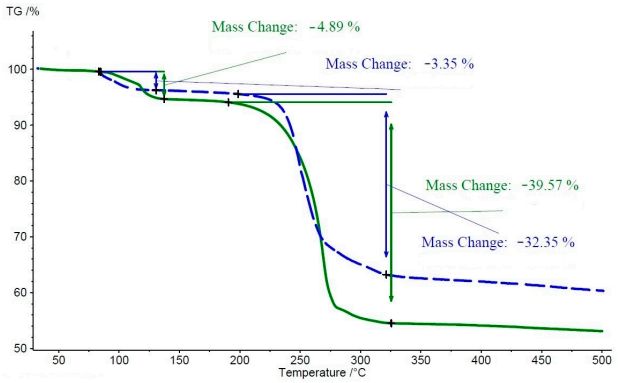

Figure 12. Thermogravimetric diagrams of the thermal decomposition of compound (**I**) (blue) and compound (**II**) (green).

While the TG diagram displays a similar thermal decomposition pattern for both compounds, the DSC analysis (Figure 13) reveals differences in the thermal behavior of compound (**I**) and compound (**II**) prior to their final decomposition. As was previously visible in the TG analysis, both compounds release water at temperatures lower than 100 °C with onset points of 87 and 74 °C for compounds (**I**) and (**II**), respectively. After this step, compound (**I**) shows a visible phase change in the range from 107 to 122 °C with three distinct peaks in the heating phase (107, 121, and 126 °C). In the cooling phase, only two peaks are visible (109 and 122 °C), however. Since compound (**II**) does not show any phase change, this transformation might be related to motions of the nitrate group. The energy release patterns in the DSC for both compounds are relatively alike, and a broad peak appears from 220 to 300 °C with one big peak and a shoulder next to it in the final stage of decomposition. The diagram of energy release in the DSC is again more similar to the decomposition of $(N_2H_5)_2[B_{12}H_{12}] \cdot 2\ N_2H_4$ rather than to the cesium-hydroborate *anti*-perovskites with oxoanions. There is a notable difference in thermal behavior of compounds (**I**) and (**II**) to other energetic compounds of the dodecahydro-*closo*-dodecaborate family, such as the diguanidinium [37] and the dihydrazinium compounds visible [16], since the mentioned examples always show a small endothermic peak right before thermally decomposing, which can be assigned as activation energy, but in the newly synthesized compounds (**I**) and (**II**), this phenomenon is not observable. The DSC analyses also revealed the amount of energy release from these compounds, which is around 1340 J/g (= 430 kJ/mol) and 2130 J/g (= 760 kJ/mol) for compounds (**I**) and (**II**), respectively. These numbers compare well with the cesium-oxoanion *anti*-perovskites with $[B_{12}H_{12}]^{2-}$ clusters, showing a bit of an increase in terms of energy release (1175 and 1950 J/g for $Cs_3[NO_3][B_{12}H_{12}]$ and $Cs_3[ClO_4][B_{12}H_{12}]$, respectively). The TG and DSC diagrams indicate that the removal of water molecules from these compounds can be achieved without causing their damage or thermal decomposition. However, it is important to note that the crystallinity of both compounds is lost during this process. As a result, the compounds become unsuitable for any single-crystal X-ray diffraction analysis.

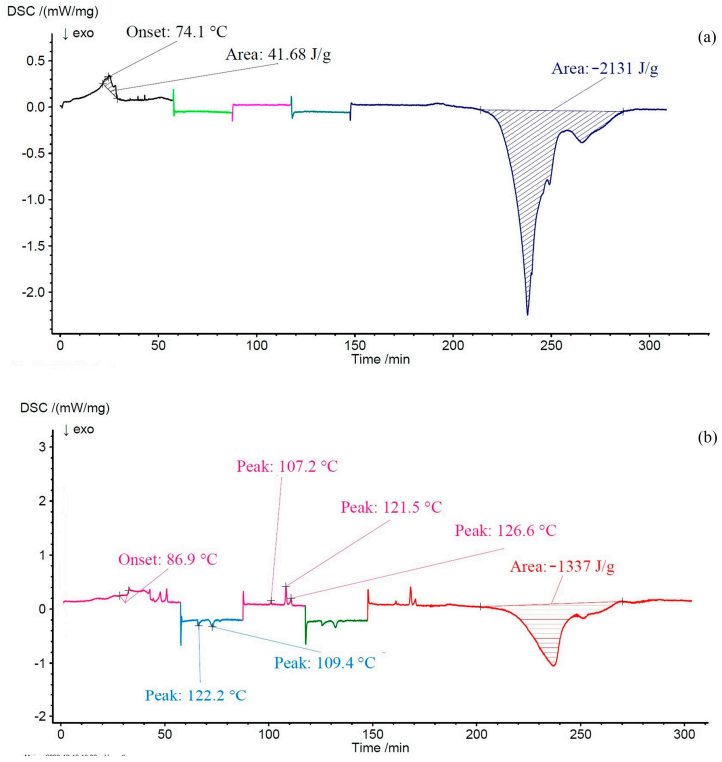

Figure 13. DSC curves of the phase change and the thermal decomposition of $(N_2H_5)_3[ClO_4][B_{12}H_{12}] \cdot H_2O$ (**II**) (**a**) and $(N_2H_5)_3[NO_3][B_{12}H_{12}] \cdot H_2O$ (**I**) (**b**).

4. Conclusions

In this research, crystals of two new energetic compounds with empirical formulae $(N_2H_5)_3X[B_{12}H_{12}] \cdot H_2O$, where X^- is either $[NO_3]^-$ or $[ClO_4]^-$, were synthesized. Single-crystal X-ray analyses show both orthorhombic compounds to have the same space group, namely $Cmc2_1$, and quite similar unit-cell parameters ($(N_2H_5)_3[NO_3][B_{12}H_{12}] \cdot H_2O$: a = 915.94(5) pm, b = 1817.45(9) pm, c = 952.67(5) pm, and $(N_2H_5)_3[ClO_4][B_{12}H_{12}] \cdot H_2O$: a = 1040.51(6) pm, b = 1757.68(9) pm, c = 942.34(5) pm, both for Z = 4). The change in the molar volume from V_m = 238.8(1) $cm^3\ mol^{-1}$ for the nitrate- to V_m = 259.5(1) $cm^3\ mol^{-1}$ for the perchlorate-containing compound nicely reflects the replacement of a $[NO_3]^-$ with a $[ClO_4]^-$ anion [38]. Further crystallographic investigations show the two compounds, though heavily distorted by the presence of the water molecules in their structure, to still exhibit hexagonal *anti*-perovskite structures, so each X^- anion ($[NO_3]^-$ or $[ClO_{4]}{}^-$) is surrounded by six hydrazinium cations, which create a distorted octahedral coordination sphere, and these octahedra share *trans*-oriented faces along the crystallographic [001] direction. The resulting pillars are bundled like a hexagonal rod-packing and held together by the bulky $[B_{12}H_{12}]^{2-}$ anions. A thermal analysis of these compounds shows that they are capable of releasing energy up to 760 kJ/mol.

Supplementary Materials: The following supporting information can be downloaded at: https://www.mdpi.com/article/10.3390/cryst14040310/s1, Table S1: (Fractional atomic coordinates and coefficients of the equivalent isotropic displacement parameters for $(N_2H_5)_3[NO_3][B_{12}H_{12}] \cdot H_2O$ (**I**)); Table S2: (Fractional atomic coordinates and coefficients of the equivalent isotropic displacement parameters for $[N_2H_5]_3[ClO_4][B_{12}H_{12}] \cdot H_2O$ (**II**)); Figure S1: (Powder X-ray diffraction pattern of $(N_2H_5)_3[NO_3][B_{12}H_{12}] \cdot H_2O$ (**I**) (top) and the calculated pattern (bottom)); Figure S2: (Powder X-ray diffraction pattern of $(N_2H_5)_3[ClO_4][B_{12}H_{12}] \cdot H_2O$ (**II**) (top) and the calculated pattern (bottom)). Figure S3: (Illustration of the classical hydrogen-bond system in $(N_2H_5)_3[ClO_4][B_{12}H_{12}] \cdot H_2O$ (**II**) with six hydrogen atoms for hydrazinium 2).

Author Contributions: Research, R.A.H.; analysis, R.A.H.; writing, R.A.H.; supervision, T.S.; correction, T.S.; revision and advice over energetic parts, T.M.K. All authors have read and agreed to the published version of the manuscript.

Funding: The Federal State of Baden-Württemberg and this research received no external funding.

Data Availability Statement: The original contributions presented in the study are included in the article/Supplementary Materials; further inquiries can be directed to the corresponding author/s.

Acknowledgments: We thank Falk Lissner for measuring the single-crystal X-ray diffraction data and Christof Schneck for his help during our thermal analyses and Barbara Förtsch for measuring our elemental analyses.

Conflicts of Interest: The authors declare no conflicts of interest.

References

1. Klapötke, T.M. *Chemistry of High-Energy Materials*; Walter de Gruyter GmbH & Co KG: Berlin, Germany, 2022.
2. Zawadzka-Małota, I. Testing of Mining Explosives with Regard to the Content of Carbon Oxides and Nitrogen Oxides in Their Detonation Products. *J. Sustain. Min.* **2015**, *14*, 173–178. [CrossRef]
3. Isobe, D.; Jiang, R. Explosive Demolition Planning of Building Structures Using Key Element Index. *J. Build. Eng.* **2022**, *59*, 104935. [CrossRef]
4. Pang, W.; Klapötke, T.M.; DeLuca, L.T.; OuYang, D.; Qin, Z.; Hu, Y.; Fan, X.; Zhao, F. Effects of TKX-50 on the Performance of Solid Propellants and Explosives. *Nano Micro-Scale Energ. Mater. Propellants Explos.* **2023**, *1*, 149–190.
5. Galante, E.; Haddad, A.; Marques, N. Application of Explosives in the Oil Industry. *Int. J. Oil Gas Coal Eng.* **2013**, *1*, 16–22. [CrossRef]
6. Steinhauser, G.; Klapötke, T.M. "Green" Pyrotechnics: A Chemists' Challenge. *Angew. Chem. Int. Ed.* **2008**, *47*, 3330–3347. [CrossRef] [PubMed]
7. Zhu, S.; Wu, Y.; Zhang, W.; Mu, J. Evaluation of a New Primary Explosive: Nickel Hydrazine Nitrate (NHN) Complex. *Propellants Explos. Pyrotech.* **1997**, *22*, 317–320.
8. Davis, S.M.; Yilmaz, N. Advances in Hypergolic Propellants: Ignition, Hydrazine, and Hydrogen Peroxide Research. *Adv. Aerosp. Eng.* **2014**, *2014*, 729313. [CrossRef]

9. Karaghiosoff, K.; Klapötke, T.M.; Sabaté, C.M. Nitrogen-Rich Compounds in Pyrotechnics: Alkaline-Earth Metal Salts of 5,5′-Hydrazine-1, 2-diylbis(1H-tetrazole). *Eur. J. Inorg. Chem.* **2009**, *2*, 238–250. [CrossRef]
10. Niemeier, J.K.; Kjell, D.P. Hydrazine and Aqueous Hydrazine Solutions: Evaluating Safety in Chemical Processes. *Org. Proc. Res. Dev.* **2013**, *17*, 1580–1590. [CrossRef]
11. Xia, Y.; Sun, J.; Mao, Z.; Hong, Z.; Kang, B. Crystal Structure of Hydrazine Nitrate. *Energ. Mater.* **2008**, *16*, 73–77.
12. Conant, J.W.; Roof, R.B. The Crystal Structures of the Isostructural Compounds Hydrazinium Fluoroborate and Hydrazinium Perchlorate. *Acta Crystallogr.* **1970**, *26*, 1928–1932. [CrossRef]
13. Wunderlich, J.A.; Lipscomb, W.N. Structure of $B_{12}H_{12}^{2-}$ Ion. *J. Am. Chem. Soc.* **1960**, *82*, 4427–4428. [CrossRef]
14. Sivaev, I.B.; Bregadze, V.I.; Sjöberg, S. Chemistry of *closo*-Dodecaborate Anion $[B_{12}H_{12}]^{2-}$: A Review. *Collect. Czech. Chem. Commun.* **2002**, *67*, 679–727. [CrossRef]
15. Tiritiris, I. Untersuchungen zu Reaktivität, Aufbau und Struktureller Dynamik von Salzartigen *closo*-Dodekaboraten. Ph.D. Thesis, University of Stuttgart, Stuttgart, Germany, 2004.
16. Zimmermann, L.W.; Aghaei Hakkak, R.; Ranjbar, M.; Schleid, T. Crystal Structures and Thermal Analyses of Three New High-Energy Hydrazinium Hydro-*closo*-Borates. *Int. J. Hydrogen Energy* **2024**, *49*, 1469–1477. [CrossRef]
17. Derdziuk, J.; Malinowski, P.J.; Jaroń, T. Synthesis, Structural Characterization and Thermal Decomposition Studies of $(N_2H_5)_2B_{12}H_{12}$ and Its Solvates. *Int. J. Hydrogen Energy* **2019**, *44*, 27030–27038. [CrossRef]
18. Wenk, H.-R.; Bulakh, A. *Minerals: Their Constitution and Origin*; Cambridge University Press: Cambridge, UK, 2016.
19. Zhang, L.; Mei, L.; Wang, K.; Lv, Y.; Zhang, S.; Lian, Y.; Liu, X.; Ma, Z.; Xiao, G.; Liu, Q. Advances in the Application of Perovskite Materials. *Nano-Micro Lett.* **2023**, *15*, 177. [CrossRef] [PubMed]
20. Kirmani, A.R.; Ostrowski, D.P.; VanSant, K.T.; Byers, T.A.; Bramante, R.C.; Heinselman, K.N.; Tong, J.; Stevens, B.; Nemeth, W.; Zhu, K. Metal Oxide Barrier Layers for Terrestrial and Space Perovskite Photovoltaics. *Nat. Energy* **2023**, *8*, 191–202. [CrossRef]
21. Souri, M.; Amoli, H.S. Gas Sensing Mechanisms in ABO_3 Perovskite Materials at Room Temperature: A Review. *Mater. Sci. Semicond. Process.* **2023**, *156*, 107271. [CrossRef]
22. Li, X.; Zhang, Y.; Kang, W.; Yan, Z.; Shen, Y.; Huo, J. Anti-Perovskite Nitrides and Oxides: Properties and Preparation. *Comput. Mater. Sci.* **2023**, *225*, 112188. [CrossRef]
23. Bareiß, K.U.; Bette, S.; Enseling, D.; Jüstel, T.; Schleid, T. Extraordinary Intense Blue Tl^+ Lone-Pair Photoluminescence from Thallium(I) Chloride Hydroborate $Tl_3Cl[B_{12}H_{12}]$. *Dalton. Trans.* **2022**, *51*, 13331–13341. [CrossRef]
24. Tiritiris, I.; Weidlein, J.; Schleid, T. Dodekahydro-*closo*-Dodekaborat-Halogenide der schweren Alkalimetalle mit der Formel $M_3X[B_{12}H_{12}]$ (M = K–Cs, NH_4; X = Cl und Br)/Dodecahydro-*closo*-Dodecaborate Halides of the Heavy Alkali Metals with the Formula $M_3X[B_{12}H_{12}]$ (M = K–Cs, NH_4; X = Cl and Br). *Z. Naturforschung B* **2005**, *60*, 627–639. [CrossRef]
25. Schouwink, P.; Sadikin, Y.; van Beek, W.; Černý, R. Experimental Observation of Polymerization from BH_4^- to $B_{12}H_{12}^{2-}$ in Mixed-Anion $A_3BH_4B_{12}H_{12}$ (A = Rb^+, Cs^+). *Int. J. Hydrogen Energy* **2015**, *40*, 10902–10907. [CrossRef]
26. Aghaei Hakkak, R.; Tiritiris, I.; Schleid, T. Synthesis and Characterization of High-Energy *Anti*-Perovskite Compounds $Cs_3X[B_{12}H_{12}]$ Based on Cesium Dodecahydro-*closo*-Borate with Molecular Oxoanions (X^- = $[NO_3]^-$, $[ClO_3]^-$ and $[ClO_4]^-$). *Molecules* **2024**, *29*, 382. [CrossRef] [PubMed]
27. Chen, S.; Shang, Y.; Jiang, J.; Huang, M.; Ren, J.; Guo, T.; Yu, C.; Zhang, W.; Chen, X. A New Nitrate-Based Energetic Molecular Perovskite as a Modern Edition of Black Powder. *Energ. Mater. Front.* **2022**, *3*, 122–127. [CrossRef]
28. Zhou, J.; Ding, L.; Zhao, F.; Wang, B.; Zhang, J. Thermal Studies of Novel Molecular Perovskite Energetic Material $(C_6H_{14}N_2)[NH_4(ClO_4)_3]$. *Chin. Chem. Lett.* **2020**, *31*, 554–558. [CrossRef]
29. Zhou, J.; Zhang, J.; Chen, S.; Zhao, F.; Qiu, L.; Meng, Z.; Ding, L.; Wang, B.; Pan, Q. Comparative Thermal Research on Energetic Molecular Perovskite Structures. *Molecules* **2022**, *27*, 805. [CrossRef] [PubMed]
30. Sheldrick, G.M. *SHELXS-97 and SHELXL-97, Program for Crystal Structure Solution and Refinement*; University of Göttingen: Göttingen, Germany, 1997.
31. Sheldrick, G.M. A Short History of SHELX. *Acta Crystallogr.* **2008**, *64*, 112–122. [CrossRef] [PubMed]
32. Sass, R.L.; Vidale, R.; Donohue, J. Interatomic Distances and Thermal Anisotropy in Sodium Nitrate and Calcite. *Acta Crystallogr.* **1957**, *10*, 567–570. [CrossRef]
33. Fugel, M.; Malaspina, L.A.; Pal, R.; Thomas, S.P.; Shi, M.W.; Spackman, M.A.; Sugimoto, K.; Grabowsky, S. Revisiting a Historical Concept by Using Quantum Crystallography: Are Phosphate, Sulfate and Perchlorate Anions Hypervalent? *Chem. Eur. J.* **2019**, *25*, 6523–6532. [CrossRef]
34. Muller, P.; Herbst-Irmer, R.; Spek, A.; Schneider, T.; Sawaya, M. *Crystal Structure Refinement: A Crystallographer's Guide to SHELXL*; OUP Oxford: Oxford, UK, 2006; Volume 8.
35. Fontana, M.D.; Mabrouk, K.B.; Kauffmann, T.H. Raman Probe of Pollutants in Water: Measurement Process. In Proceedings of the 4th Imeko TC19 Symposium on Environmental Instrumentation and Measurements Protecting Environment, Climate Changes and Pollution Control, IMEKO, Budapest, Hungary, 3–4 June 2013; pp. 27–29.
36. Zapata, F.; García-Ruiz, C. The Discrimination of 72 Nitrate, Chlorate and Perchlorate Salts Using IR and Raman Spectroscopy. *Spectrochim. Acta* **2018**, *189*, 535–542. [CrossRef]

37. Aghaei Hakkak, R.; Schleid, T. Crystal Structure and Thermal Behavior of Three Potential High-Energy Compounds of Hydro-*closo*-Borates with Guanidinium. *J. Solid State Chem.* **2024**, *329*, 124416. [CrossRef]
38. Simoes, M.C.; Hughes, K.J.; Ingham, D.B.; Ma, L.; Pourkashanian, M. Estimation of the Thermochemical Radii and Ionic Volumes of Complex Ions. *Inorg. Chem.* **2017**, *56*, 7566–7573. [CrossRef] [PubMed]